CHEMISTRY OF MATERIALS

pubs.acs.org/cm Article

Photo-Crosslinkable Naphthalene Diimide Polymer for Solution-Processed *n*−*i*−*p* Perovskite Solar Cells

Published as part of Chemistry of Materials virtual special issue "In Honor of Prof. Elsa Reichmanis".

Yangwei Shi,[∇] Declan P. McCarthy,[∇] Dominique Lungwitz, Fangyuan Jiang, Margherita Taddei, Hannah Contreras, Yujing Lin, Aiswarya Abhisek Mohapatra, Kan Tang, Yadong Zhang, Stephen Barlow, Antoine Kahn, Seth R. Marder,* and David S. Ginger*

Cite This: *Chem. Mater.* 2024, 36, 795−802 **Read Online**

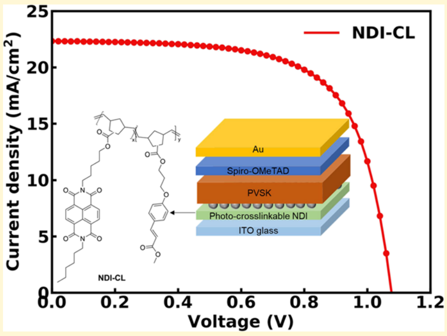

ABSTRACT: We copolymerize a norbornene monomer bearing a pendant naphthalene diimide with a norbornene bearing a cinnamate pendant moiety to synthesize a crosslinkable electron-transporting polymer and study its use in solution-processed *n*−*i*−*p* perovskite solar cells. The crosslinked material exhibits over 90% transparency in the visible region and higher thermal stability (>300 °C) and lower surface energy than the corresponding homopolymer of the naphthalene diimide functionalized norbornene. Coating an ITO surface with the photo-crosslinked copolymer yields a slightly lower work function than homopolymer-coated ITO. We show that the morphologies of the perovskite films deposited on both polymers are similar (∼300 nm features) based upon scanning electron microscopy. Our solar-cell device results show that the crosslinked naphthalene diimide polymer gives a higher open-circuit voltage (1.08 vs 1.05 V), fill factor (average 64.43 vs 58.77%), and stabilized power conversion efficiency (12.28 vs 10.33%) compared to its non-crosslinked homopolymer counterpart, as well as reduced hysteresis. We attribute the improved performance to decreased work function, reduced nonradiative recombination, and higher shunt resistance.

■ INTRODUCTION

Hybrid organic−inorganic lead halide perovskite solar cells are a rapidly emerging photovoltaic technology that has reached power conversion efficiencies (PCEs) exceeding 26%.[1] Typically perovskite solar cells incorporate transport layers between the perovskite absorber and the charge-collecting electrodes to improve carrier selectivity. Metal-oxide-based electrontransport layers (ETLs) have been widely used in *n*−*i*−*p* perovskite solar cells for a variety of reasons including their moderate to high electron mobilities, good energy alignment with the perovskite conduction band, and wide bandgaps that reduce parasitic absorption and offer hole-blocking capability.[2,3] TiO_2 remains the most common ETL used in state-of-the-art *n*−*i*−*p* cells but requires high processing temperatures and exhibits photoinstability.[4]

Organic electron transport materials represent a possible alternative to metal oxides. Organic semiconductors offer processing flexibility, tunable energy level alignment, and may offer decreased nonradiative recombination losses at the electron-extraction interface.[5,6] Of the existing organic semiconductor ETLs, fullerenes have been widely adopted and have produced efficient devices in both normal (*n*−*i*−*p*)[7] and more commonly in inverted (*p*−*i*−*n*) architectures.[8] Fullerenes offer good charge-transport properties but have poor solubility and suboptimal transparency in the visible. Furthermore, fullerenes can be a substantial source of interfacial recombination losses,[6,9] and devices incorporating fullerenes as ETLs can suffer from issues of long-term stability.[10,11]

Alternative nonfullerene organic ETLs have been employed as small molecules and polymers including perylene diimides,[12,13] naphthalene diimides,[14−16] and azaacenes.[17,18] Herein, we pursue the strategy of crosslinkable naphthalene diimide-based electron transport layers. We chose naphthalene diimides because they possess high transparency throughout the visible region and electron affinities comparable with those of perovskites combined with high hole-blocking ionization energies, and, in some cases, good electron transport properties.[19] Furthermore, the synthesis of naphthalene diimides is straightforward and can be readily modified to tune both their solubility and electron affinity via substitution at the imide and naphthalene core positions.[20] Naphthalene

Received: September 7, 2023
Revised: December 19, 2023
Accepted: December 20, 2023
Published: January 9, 2024

https://doi.org/10.1021/acs.chemmater.3c02295

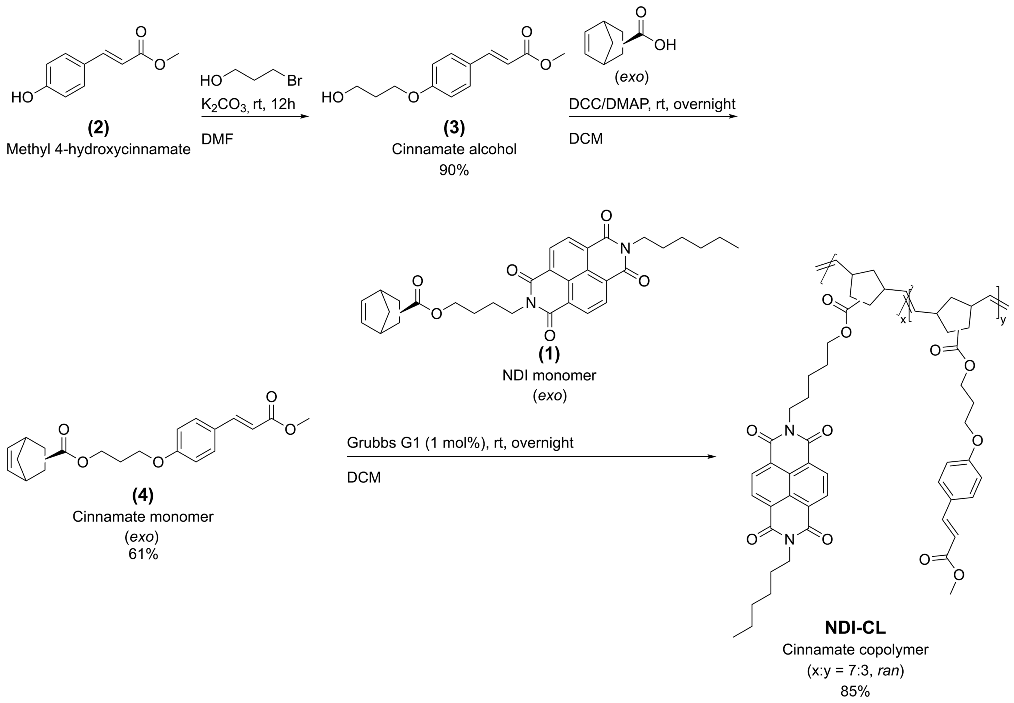

Figure 1. Synthesis and molecular structure of NDI-1 and the cinnamate copolymer (NDI-CL).

diimide acceptors have been incorporated in a number of polymeric architectures for various applications in organic electronics[21] but less widely in perovskite photovoltaics.

Herein, we also focus on crosslinking the naphthalene diimide-based ETLs because crosslinking offers many possible processing and stability advantages. For example, crosslinked charge transport layers can be used to increase the robustness of derived organic electronic devices toward degradation.[17,22,23] Crosslinking also imparts solvent resistance, which can allow for the deposition of subsequent layers from solution in nonorthogonal solvents.[2] Numerous crosslinking approaches have been used for transport layers in the literature.[24] Here, we chose a copolymerization strategy incorporating a cinnamate containing comonomer. The cinnamate functional group is relatively easily incorporated into monomers bearing a polymerizable group and is compatible with a wide range of polymerization methods.[25] Cinnamates are particularly attractive crosslinking groups because they undergo selective dimerization, avoiding the need for an added photoinitiator and preventing unwanted functionalization of electroactive portions of the polymer.[26] Additionally, they are tolerant of molecular redox dopants, allowing for doping before or after insolubilization. Crosslinking can be achieved via mild photoirradiation with a handheld UV lamp.[27−29] Photo-crosslinking offers advantages compared to thermal crosslinking as the process does not require high temperature annealing and thus can be used on plastic substrates or in top (rear) charge selective contacts without degrading the underlying perovskite layer.

Developing new nonfullerene organic ETLs for perovskite solar cells remains a considerable challenge. The Marder and Bach groups previously reported the use of a naphthalene diimide side chain homopolymer that achieved stabilized PCEs of >13.5% in *n*−*i*−*p* perovskite solar cells.[30] Here, we report the synthesis, characterization, and material properties of a related new copolymer (NDI-CL) which incorporates cinnamate crosslinking groups. We demonstrate this polymer's high transparency, thermal stability, photo-crosslinking, and n-doping via solution and sequential processing. We demonstrate its applicability in perovskite solar cells through characterization of solar cell device performance relative to its uncrosslinked homopolymeric counterpart (NDI-1) in *n*−*i*−*p* devices with an MA-free perovskite absorber (MA = methylammonium).

■ RESULTS AND DISCUSSION

Figure 1 shows the polymer structures and their syntheses. The naphthalene diimide monomer (**1**) and the corresponding homopolymer (NDI-1, see Figure S1 for its molecular structure) were synthesized for this work (M_n = 54.5 kDa, $Đ$ = 1.50) following methods previously reported.[30] The cinnamate norbornene monomer was synthesized over two steps (Figure S2): the commercially available methyl 4-hydroxycinnmate (**2**) was etherified to methyl 4-(3-hydroxypropoxy)cinnamate (**3**) by deprotonation with anhydrous potassium carbonate and alkylation with 3-bromo-1-propanol in *N,N*-dimethylformamide (DMF). The norbornene cinnamate monomer (**4**) was then synthesized by a Steglich esterification with *exo*-5-norbornenecarboxylic acid using dicyclohexylcarbodiimide (DCC) and catalytic 4-dimethylaminopyridine (DMAP). The polymer (NDI-CL) was synthesized by ring-opening metathesis polymerization (ROMP) of the naphthalene diimide monomer and cinnamate monomer in a 7:3 ratio (Figure S5), respectively, with a Grubbs first generation catalyst in dichloromethane (DCM) (M_n = 45.4 kDa, $Đ$ = 1.17). The SEC (GPC) traces of both polymers in chloroform are shown in Figure S7. The polymer exhibited good solubility in low polarity solvents commonly used in device processing such as chloroform, chlorobenzene, and dichlorobenzene.

We characterized the optical properties and crosslinking of thin films of NDI-CL cast from chlorobenzene. The UV−vis

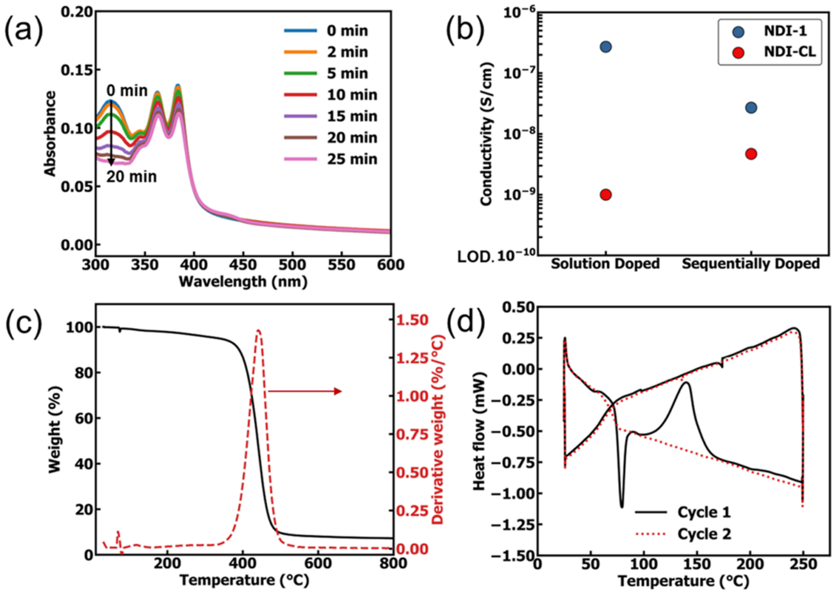

Figure 2. (a) UV−vis absorption spectrum of NDI-CL film on glass with increasing irradiation time with 365 nm hand-held UV lamp. (b) Conductivity of solution and sequentially doped NDI-1 and NDI-CL films; LOD represents limit of detection. (c) Thermogravimetric analysis (TGA) of NDI-CL polymer and derivative weight. (d) Differential scanning calorimetry of NDI-CL polymer.

absorption spectrum of NDI-CL prior to crosslinking shows a vibronically structured feature similar to that of small-molecule unsubstituted NDIs (Figure 2a),[20] with a broad unstructured absorption peaking at ca. 310 nm attributable to the absorption of the *para*-alkoxy-substituted cinnamate moiety.[28] We then photoirradiated the films at 365 nm with a hand-held UV lamp for 25 min; the observed changes in the absorption spectrum over time—the absorbance of the cinnamate feature decreases to reach a near minimum after *ca*. 20 min irradiation (Figure 2a)—which we attribute to the [2 + 2] cycloaddition reaction of the cinnamate. Subsequently, in Figure S9, we demonstrate the solvent resistance of the films toward both the casting solvent and the perovskite ink solvent mixture, chlorobenzene, and 4:1 DMF:DMSO (DMSO = dimethyl sulfoxide), respectively, by spin coating each solvent atop the crosslinked films and showing negligible changes in the absorption spectrum.

Once we had established an effective crosslinking protocol, we sought to investigate the charge-transport properties of these materials. In the absence of doping, the conductivities were below the limit of detection ($<10^{-10}$ S/cm) of our apparatus. We used the highly reducing but moderately air-stable dimeric benzimidazole dopant, $(\text{N-DMBI})_2$, as a reducing agent.[31] Solution doping was carried out on NDI-1 (9 mol % dimeric dopant) without the addition of a crosslinker. Solution doping of the copolymer (9 mol % dimeric dopant) was followed by crosslinking. We also investigated a sequential doping protocol where a dopant solution (6 mg/mL) was applied to the crosslinked film followed by chlorobenzene washing step. For sequential doping, NDI-1 was cross-linked by 5% weight addition of an oligomeric azide crosslinker, 4Bx, shown in Figure S1, followed by photoirradiation at 254 nm for 5 min.[32] Figure 2b shows that all polymer dopant systems exhibit modest conductivities (10^{-9}−10^{-6} S/cm). Additionally, solution-doped NDI-1 exhibited better conductivity by several orders of magnitude compared to the solution-doped and crosslinked NDI-CL. Sequentially-doped and crosslinked NDI-CL had slightly better conductivity than its solution-doped and crosslinked counterpart, perhaps because the polymer morphology was less interrupted by the doping process. In summary, doping of these side chain naphthalene diimide polymers improves their conductivity, but only achieving values of 10^{-9}−10^{-6} S/cm, which is less than other state-of-the-art n-doped electron-transporting polymers, which can reach conductivities of 1.1×10^{-3} S/cm.[33]

We also characterized the thermal properties of NDI-CL (without photo-crosslinking) by thermogravimetric analysis (TGA) and differential scanning calorimetry (DSC), shown in Figure 2c,d, respectively. The TGA indicates the decomposition temperature of the polymer, T_d, defined as temperature at which 5% of mass is lost, is ca. 335 °C. The first DSC cycle shows a small endotherm around 80 °C which likely reflects loss of the trapped solvent (note in Figure S6 trace of DCM present according to ^{1}H NMR spectroscopy). Additionally, a melting peak is observed around 135 °C in the first cycle. However, after the thermal history of the polymer has been cleared, we observe no transitions up to 200 °C in the second cycle. The excellent thermal stability of the polymer implies compatibility with high temperature annealing steps for the deposition of other layers in perovskite solar cell devices.

We dissolved NDI-1 and NDI-CL in anhydrous chlorobenzene to form solutions with a concentration of 1 mg/mL prior to spin coating onto the ITO substrates. The thickness of the NDI polymer films was estimated to be ∼4 nm using atomic force microscopy (AFM) measurements (Figure S10). In addition, the naphthalene diimide polymers cover the ITO substrate conformally (Figure S10b). We further measured the work function of NDI-1 and crosslinked NDI-CL modified ITO using scanning Kevin probe microscopy (SKPM) with highly oriented pyrolytic graphite (HOPG) as the reference. We obtain uniform and homogeneous surface potential distributions with both NDI-1 and NDI-CL layers, which is beneficial for the charge collection at the interface (Figure S11).[34] We measured the work function of NDI-CL/ITO to be ∼4.36 eV, which is lower than that of NDI-1/ITO (∼4.55 eV),

https://doi.org/10.1021/acs.chemmater.3c02295
Chem. Mater. 2024, 36, 795−802

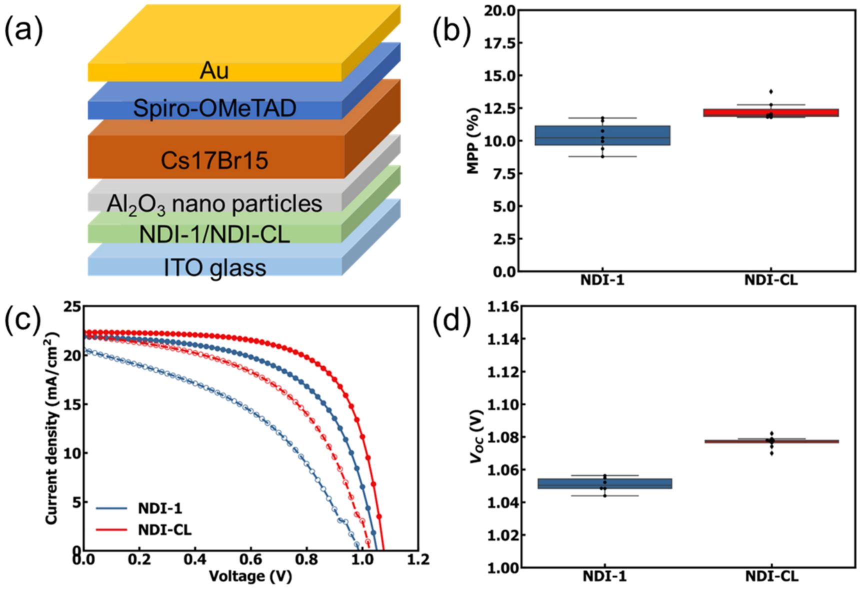

Figure 3. (a) Device structure used in this study (*n*−*i*−*p*). (b) Statistical distribution of the stabilized maximum power point (MPP). (c) Characteristic *J*−*V* curves (solid dots indicate reverse scan and hollow dots indicate forward scan) of perovskite solar cells based on NDI-1 and NDI-CL ETLs. (d) Statistical distribution of V_{OC} values obtained from reverse scans.

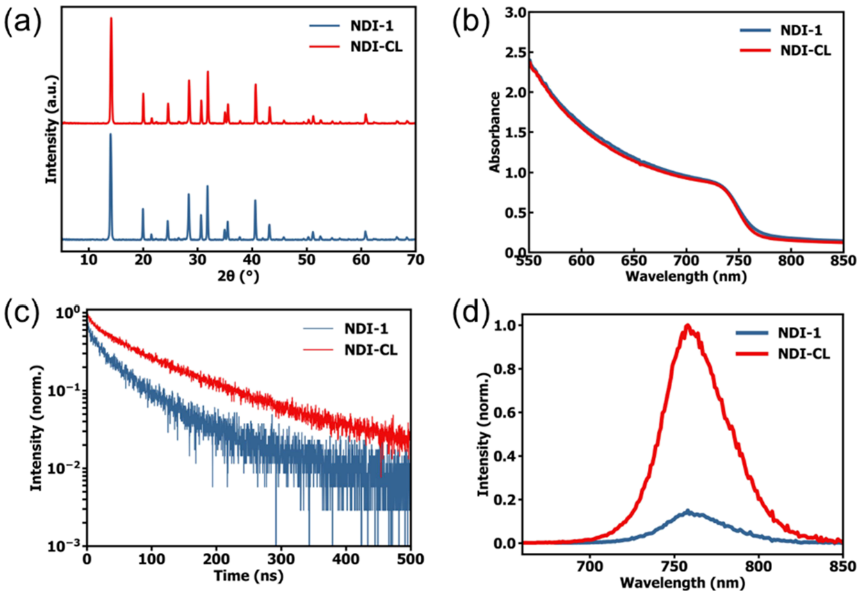

Figure 4. (a) XRD patterns, (b) UV−vis absorption spectra, (c) time-resolved PL (excited from ITO side with 640 nm laser), and (d) steady-state PL emission (excited from ITO side with 640 nm wavelength) of Cs17Br15 coated on NDI-1 and NDI-CL.

and similar to NDI-modified ITO in a previous report.[35] We performed drift-diffusion simulations with Solar Cell Capacitance Simulator (SCAPS)[36,37] to understand the impact of the reduced work function of the electron-collecting electrode on the perovskite solar cell's performance. We varied the work function of the electron-collecting electrode and found that the reduced work function will, in theory, increase the device V_{OC} (Figure S12).

To compare device performance, we focused our analysis on the mixed-cation mixed-halide perovskite $FA_{0.83}Cs_{0.17}Pb(I_{0.83}Br_{0.15})_3$ (we denote as Cs17Br15, FA^+ = formamidinium), which has a bandgap of 1.63 eV.[9] Figure 3a shows the *n*−*i*−*p* device architecture used in this study. As in the previous study of NDI-1, we utilized a sparse dispersion of Al_2O_3 nanoparticles on top of the naphthalene diimide polymers to improve wettability and obtain continuous perovskite films as the neat films of both polymers were hydrophobic (Figure S13).[38] The Al_2O_3 nanoparticles should only cover partial of the surface area of the polymers and help improve wetting.[39]

We used Spiro-OMeTAD as the hole transport layer (HTL) and gold (Au) as the top electrode. Figure 3c shows the characteristic *J*−*V* curves for NDI-1 and NDI-CL devices under 1 sun illumination and clearly indicates that the device using NDI-CL gives a higher V_{OC} than using NDI-1, as expected based on the work-function measurement. In addition, NDI-CL also reduces device hysteresis. We fabricated devices with SnO_2 as the ETL (Figure S14a) and without an ETL (Figure S14b). The two devices also showed hysteresis, indicating that the hysteresis might be associated with the perovskite layer or perovskite/Spiro-OMeTAD interface. We

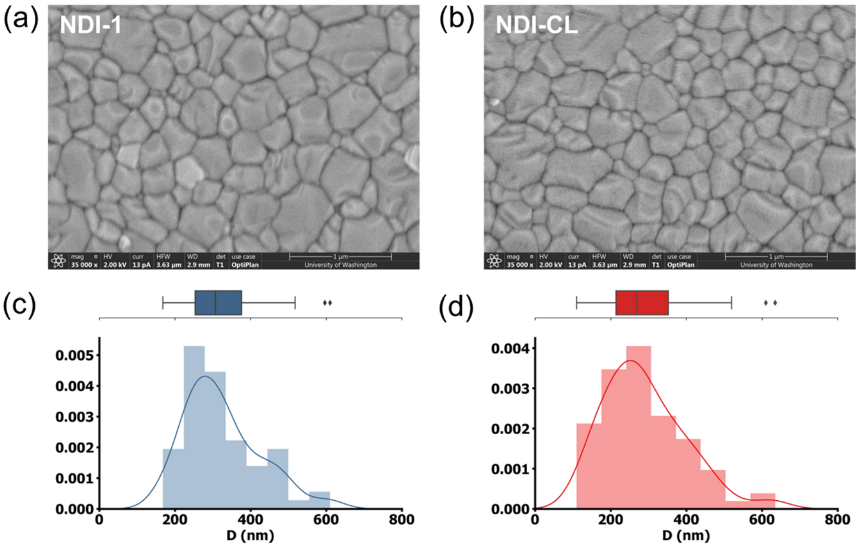

Figure 5. Top view SEM images of perovskite Cs17Br15 on (a) NDI-1- and (b) NDI-CL-modified ITO substrates. Corresponding grain size distributions of perovskite Cs17Br15 on (c) NDI-1- and (d) NDI-CL-modified ITO substrates.

measure a maximum V_{OC} of ~1.08 V for the NDI-CL solar cell. Figure 3b,d shows the statistical distribution of maximum power point (MPP) and V_{OC} with all other photovoltaic parameters summarized in Table S1 and Figure S15. Overall, when using the crosslinked polymer, we see a consistent increase of V_{OC} (~30 mV on average) and FF and thus PCE based on the reverse scan. The enhanced V_{OC} in NDI-CL-based solar cell devices is qualitatively consistent with the predictions from our SCAPS drift-diffusion simulations. We speculate that the enhanced FF might also be due to crosslinked NDI-CL blocking the shunting path between the perovskite and the ITO electrode or reduced nonradiative recombination at the polymer/perovskite interface (see below). We measured the dark $J-V$ curve of NDI-1 and NDI-CL devices as shown in Figure S16. The NDI-CL solar cell device exhibits a better diode characteristic with reduced leakage current density and a higher rectification ratio compared to the NDI-1 device.[40] This indicates that the NDI-CL solar cell device has higher shunt resistance[41] and a suppression of charge carrier recombination in the device compared to the NDI-1 solar cell device.[42] Based on the lumped equivalent circuit model,[43] we estimate the shunt resistance of the NDI-CL-based perovskite solar cell to be 5270 ± 350 $\Omega\cdot cm^2$, which is double that of the NDI-1-based device (2210 ± 210 $\Omega\cdot cm^2$, Figure S17). We further fitted the dark $J-V$ curve to obtain the series resistances for NDI-CL and NDI-1 devices, which are 8.5 ± 1.8 and 9.9 ± 0.8 $\Omega\cdot cm^2$, respectively. In addition, we obtain stabilized power output (SPO) efficiencies of ~12.28 and ~10.33% for solar cells using NDI-CL and NDI-1, respectively (Figure 3b and Table S1).

To understand the differences in performance between NDI-1 and NDI-CL devices, we examined the influence of NDI-1 and NDI-CL on the quality of perovskite film formation. Figure 4a shows the X-ray diffraction (XRD) patterns of perovskite Cs17Br15 on top of the NDI-1- and NDI-CL-modified ITO substrates. The peak positions, full width at half maximum (FWHM), and peak intensities are indistinguishable, and we conclude therefore that the crystallinity of perovskite Cs17Br15 remains the same. In addition, the UV−vis absorption spectra show nearly identical absorption for Cs17Br15 films deposited on the two different substrates (Figure 4b). Figure 4c,d shows the photoluminescence (PL) lifetime and PL emission of Cs17Br15 on NDI-1- and NDI-CL-modified ITO substrates. We measure a longer lifetime (~74 ns) with stretched exponential fitting for perovskite on NDI-CL-modified ITO in comparison to that on NDI-1 (~25 ns) when excited from the ITO side with a 640 nm wavelength. Accordingly, the PL emission of Cs17Br15 on NDI-CL is ~6.5 times higher than that of Cs17Br15 on NDI-1, which is consistent with an enhanced PL lifetime, suggesting a potential reduction of defect density at the bottom interface. The suppressed nonradiative recombination may be due to a chemical passivation effect of NDI-CL, or simply reduced coupling between the NDI and perovskite due to the cinnamate, which may be partially responsible for the improved device performance observed with NDI-CL, especially improvements in the V_{OC}.

The morphology and grain structure of perovskite films also play an important role in device performance.[44,45] We used scanning electron microscopy (SEM) imaging to investigate the morphology of Cs17Br15 perovskite films deposited on NDI-1- and NDI-CL-modified ITO substrates. Figure 5a,b shows top view SEM images of Cs17Br15 perovskite films on NDI-1 and NDI-CL. The perovskite films are dense and pinhole-free on both NDI-1- and NDI-CL-modified ITO substrates with smooth and clean surfaces, indicating good film quality. Figure 5c,d shows the corresponding grain size distributions for the two cases (approximating that SEM morphology corresponds to the grain structure, while acknowledging that this approximation can be inaccurate[45]). The average grain sizes obtained from the SEM images (~324 ± 99 vs ~289 ± 108 nm) are similar for Cs17Br15 perovskite on NDI-1- and NDI-CL-modified ITO substrates. The surface roughness of the perovskite film on NDI-CL-modified ITO is ~13.6 nm, slightly lower than that of perovskite on NDI-1, which is ~18.5 nm (Figure S18). A slightly smoother perovskite film on NDI-CL should also be beneficial for device performance.

CONCLUSIONS

In summary, we report a photo-crosslinkable naphthalene diimide copolymer as ETL for solution processed perovskite solar cells. The crosslinked ETL, NCI-CL, exhibits both high transparency of over 90% in the visible region and high thermal stability (~ 300 °C). NDI-CL-modified ITO shows a slightly lower work function than ITO modified with the non-crosslinked NDI-1. Our solar cell device results show that the crosslinked NDI-CL polymer leads to slightly higher V_{OC}, FF, PCE, and less hysteresis than its non-crosslinkable NDI-1 counterpart. The average V_{OC} is enhanced to ~1.08 V from ~1.05 V with stabilized PCE increasing to 12.28% from 10.33% on average. We ascribe the improved performance to the decreased work function of the NDI-CL-modified ITO, and higher shunt resistance with crosslinked naphthalene diimide polymer-based perovskite solar cells. This work demonstrates that a crosslinked polymer ETL works for perovskite solar cells, which provides insights into the design of polymer electron-transport materials for perovskite solar cells.

METHODS

Materials. All chemicals were purchased from commercial sources and used as received unless stated otherwise. Column chromatography was carried out using silica gel (46−63 μm, Sorbent) as the stationary phase, and thin-layer chromatography (TLC) was performed on precoated silica-gel plates (0.25 mm thick, 60F254, EMD, Germany) and visualized under UV light. Nuclear magnetic spectroscopy measurements were carried out on Bruker Avance III 400 or Avance III HD 500 MHz instruments and calibrated using the solvent residual as an internal reference ($CHCl_3$, 7.26 ppm ^1H NMR, 77.16 ppm ^{13}C NMR). Polymers were analyzed using a Tosoh EcoSEC HLC 8320 GPC system equipped with a TSKgel SuperHZ-L column with a $CHCl_3$ eluant containing 0.25% NEt_3 at a flow rate of 0.45 mL/min at 40 °C. All number-average molecular weights and dispersities were calculated from refractive index chromatograms using PStQuick Mp-M polystyrene standards. Elemental analyses were carried out by Atlantic Microlabs using a LECO 932 CHNS elemental analyzer.

Materials for Halide Perovskite and Perovskite Film Preparation. All precursors were used without any further purification and were stored in a nitrogen-filled glovebox. Formamidinium iodide (FAI, Greatcell), cesium iodide (CsI, Sigma), lead iodide (PbI_2, Sigma), and lead bromide ($PbBr_2$, Sigma) were dissolved in a mixture of anhydrous *N,N*-dimethylformamide (DMF, Sigma) and anhydrous dimethyl sulfoxide (DMSO, Sigma) (volume ratio of 4:1) to prepare a 1.2 M solution of $FA_{0.83}Cs_{0.17}Pb(I_{0.75}Br_{0.15})_3$ according to the stoichiometry. Patterned indium tin oxide (ITO, from thin film devices) glass substrates and glass substrates were cleaned by sequentially sonicating in water containing ~2% Micro-90 detergent, DI water, acetone, and 2-propanol (IPA) for 10 min, respectively, followed by plasma-cleaning for 5 min. The perovskite precursor solution was filtered with a PTFE filter before use, and 50 μL of the solution was deposited on top of the substrate and spin-coated at 4000 rpm for 60 s. When ~35 s remained, 120 μL of anhydrous chlorobenzene (CB, Sigma) antisolvent was dropped from the top. The perovskite films were then annealed at 100 °C for 30 s and at 150 °C for 10 min. The preparation of perovskite films was carried out in a nitrogen-filled glovebox.

Fabrication of Perovskite Solar Cells. To fabricate the Cs17Br15 devices, NDI-1 and NDI-CL were dissolved in anhydrous chlorobenzene (CB) at a concentration of 1 mg/mL, and 60 μL of the solution was deposited onto the ITO substrate before spin coating at 3000 rpm for 30 s. The NDI-CL was then put under UV (UVGL-25 Compact UV Lamp) light at 365 nm (~5 cm above the film) for 20 min to crosslink the polymer. The Al_2O_3 (Sigma) was diluted in isopropyl alcohol (IPA) with a volume ratio of 1:150, which was spin-coated at 3000 rpm for 30 s, followed by annealing at 100 °C for ~1 min. The perovskite films were deposited in the same way as that mentioned above. Spiro-OMeTAD (Xi'an Polymer light technology Corp.) was used as the hole transport layer. The HTL solution was prepared by dissolving 60 mg of Spiro-OMeTAD in 700 μL CB, with addition of 22.5 μL 4-*tert*-butylpyridine (t-BP, Sigma-Aldrich) and 15.5 μL of Li-TFSI solution (520 mg/mL in acetonitrile, ACN, Sigma-Aldrich). The 60 μL HTL solution was spin-coated on top of perovskite at 3000 rpm for 30 s in a nitrogen-filled glovebox. Subsequently, the half-stacked solar cell devices were stored in a desiccator for 24 h. To complete the device fabrication, 80 nm of Au was thermally evaporated onto the devices.

Structural and Optical Characterization. A Bruker D8 Powder X-ray diffractometer (XRD) with a high-efficiency Cu anode microfocus X-ray source and sensitive Pilatus 100 K large-area 2D detector was used to study the crystal information on perovskite films. PL emission (excited at 640 nm) was measured using an Edinburgh FLS1000 spectrometer with a xenon lamp light source. A PMT-980 detector was used for the PL measurements. SEM images were acquired by using a FEI Sirion SEM instrument at a 2 kV accelerating voltage. The sample structure was ITO/NDI/Al_2O_3/perovskite.

See the Supporting Information for more information on the synthesis and other characterizations.

ASSOCIATED CONTENT

Supporting Information

The Supporting Information is available free of charge at https://pubs.acs.org/doi/10.1021/acs.chemmater.3c02295.

Detailed synthetic procedures, NMR, cyclic voltammogram, UV−vis, contact angle, AFM images, SCAPS simulation results, and photovoltaic parameters (PDF)

AUTHOR INFORMATION

Corresponding Authors

Seth R. Marder − *Department of Chemistry, Renewable and Sustainable Energy Institute, and Department of Chemical and Biological Engineering, and Materials Science and Engineering Program, University of Colorado-Boulder, Boulder, Colorado 80309, United States;* orcid.org/0000-0001-6921-2536; Email: seth.marder@colorado.edu

David S. Ginger − *Department of Chemistry, University of Washington, Seattle, Washington 98195, United States;* orcid.org/0000-0002-9759-5447; Email: dginger@uw.edu

Authors

Yangwei Shi − *Department of Chemistry and Molecular Engineering & Sciences Institute, University of Washington, Seattle, Washington 98195, United States;* orcid.org/0000-0002-9014-7422

Declan P. McCarthy − *Department of Chemistry, University of Colorado-Boulder, Boulder, Colorado 80309, United States*

Dominique Lungwitz − *Department of Electrical and Computer Engineering, Princeton University, Princeton, New Jersey 08544, United States;* orcid.org/0000-0003-1662-2114

Fangyuan Jiang − *Department of Chemistry, University of Washington, Seattle, Washington 98195, United States*

Margherita Taddei − *Department of Chemistry, University of Washington, Seattle, Washington 98195, United States;* orcid.org/0000-0003-4122-8418

Hannah Contreras − *Department of Chemistry, University of Washington, Seattle, Washington 98195, United States;* orcid.org/0000-0002-2111-2250

Yujing Lin − *Department of Chemistry, University of Washington, Seattle, Washington 98195, United States*

Aiswarya Abhisek Mohapatra − *Renewable and Sustainable Energy Institute, University of Colorado-Boulder, Boulder, Colorado 80309, United States*
Kan Tang − *Renewable and Sustainable Energy Institute, University of Colorado-Boulder, Boulder, Colorado 80309, United States*
Yadong Zhang − *Renewable and Sustainable Energy Institute, University of Colorado-Boulder, Boulder, Colorado 80309, United States*
Stephen Barlow − *Renewable and Sustainable Energy Institute, University of Colorado-Boulder, Boulder, Colorado 80309, United States;* orcid.org/0000-0001-9059-9974
Antoine Kahn − *Department of Electrical and Computer Engineering, Princeton University, Princeton, New Jersey 08544, United States;* orcid.org/0000-0002-1612-3350

Complete contact information is available at:
https://pubs.acs.org/10.1021/acs.chemmater.3c02295

Author Contributions

[∇]Y. S. and D.P.M. contributed equally to this work.

Notes

The authors declare no competing financial interest.

ACKNOWLEDGMENTS

This work was primarily supported by the U.S. Department of Energy's Office of Energy Efficiency and Renewable Energy (EERE) under the Solar Energy Technology Office (SETO), Award Number DE-EE0008747. The electrical characterization of the polymers was supported by the U.S. National Science Foundation (ECCS-2141949). Work at Princeton University was supported in part by a grant from the Department of Energy Office of Basic Energy Sciences, Division of Materials Sciences and Engineering, Award Number DE-SC0012458. D.S.G. acknowledges salary and infrastructure support from the Washington Research Foundation, the Alvin L. and Verla R. Kwiram endowment, and the B. Seymour Rabinovitch Endowment. M.T. acknowledges funding from the Office of Naval Research (Award Number N00014-20-1-2587) for her role in time-resolved photoluminescence. H.C. was supported by the National Science Foundation Graduate Research Fellowship under Grant No. DGE-2140004 and the University of Washington Clean Energy Institute (CEI) fellowship. Part of this work was carried out at the Molecular Analysis Facility, a National Nanotechnology Coordinated Infrastructure site at the University of Washington which is supported in part by the National Science Foundation (Awards NNCI-2025489 and NNCI-1542101), the Molecular Engineering & Sciences Institute, and the Clean Energy Institute. Y.S. acknowledges the use of facilities and instrumentation supported by the U.S. National Science Foundation through the UW Molecular Engineering Materials Center (MEM-C), a Material Research Science and Engineering Center (DMR-1719797). The authors acknowledge the use of facilities and instruments at the Research Training Testbed (RTT), part of the Washington Clean Energy Testbeds system. Part of this work was conducted with instrumentation supported by the University of Washington Student Technology Fee at the RTT.

REFERENCES

(1) National Renewable Energy Laboratory. Best Research-Cell Efficiencies, 2023. https://www.nrel.gov/pv/cell-efficiency.html (accessed 2023-07-28).

(2) Lian, J.; Lu, B.; Niu, F.; Zeng, P.; Zhan, X. Electron-Transport Materials in Perovskite Solar Cells. *Small Methods* **2018**, *2* (10), No. 1800082.

(3) Lin, L.; Jones, T. W.; Yang, T. C. J.; Duffy, N. W.; Li, J.; Zhao, L.; Chi, B.; Wang, X.; Wilson, G. J. Inorganic Electron Transport Materials in Perovskite Solar Cells. *Adv. Funct. Mater.* **2021**, *31* (5), No. 2008300.

(4) Leijtens, T.; Eperon, G. E.; Pathak, S.; Abate, A.; Lee, M. M.; Snaith, H. J. Overcoming Ultraviolet Light Instability of Sensitized TiO_2 with Meso-Superstructured Organometal Tri-Halide Perovskite Solar Cells. *Nat. Commun.* **2013**, *4* (1), 2885.

(5) Jameel, M. A.; Yang, T. C. J.; Wilson, G. J.; Evans, R. A.; Gupta, A.; Langford, S. J. Naphthalene Diimide-Based Electron Transport Materials for Perovskite Solar Cells. *J. Mater. Chem. A* **2021**, *9* (48), 27170−27192.

(6) Wang, J.; Fu, W.; Jariwala, S.; Sinha, I.; Jen, A. K. Y.; Ginger, D. S. Reducing Surface Recombination Velocities at the Electrical Contacts Will Improve Perovskite Photovoltaics. *ACS Energy Lett.* **2019**, *4* (1), 222−227.

(7) Yoon, H.; Kang, S. M.; Lee, J. K.; Choi, M. Hysteresis-Free Low-Temperature-Processed Planar Perovskite Solar Cells with 19.1% Efficiency. *Energy Environ. Sci.* **2016**, *9* (7), 2262−2266.

(8) Heo, J. H.; Han, H. J.; Kim, D.; Ahn, T. K.; Im, S. H. Hysteresis-Less Inverted $CH_3NH_3PbI_3$ Planar Perovskite Hybrid Solar Cells with 18.1% Power Conversion Efficiency. *Energy Environ. Sci.* **2015**, *8* (5), 1602−1608.

(9) Shi, Y.; Rojas-Gatjens, E.; Wang, J.; Pothoof, J.; Giridharagopal, R.; Ho, K.; Jiang, F.; Taddei, M.; Yang, Z.; Sanehira, E. M.; Irwin, M. D.; Silva-Acuña, C.; Ginger, D. S. (3-Aminopropyl)Trimethoxysilane Surface Passivation Improves Perovskite Solar Cell Performance by Reducing Surface Recombination Velocity. *ACS Energy Lett.* **2022**, *7* (11), 4081−4088.

(10) Jung, S. K.; Lee, D. S.; Ann, M. H.; Im, S. H.; Kim, J. H.; Kwon, O. P. Non-Fullerene Organic Electron-Transporting Materials for Perovskite Solar Cells. *ChemSusChem* **2018**, *11* (22), 3882−3892.

(11) Warby, J.; Zu, F.; Zeiske, S.; Gutierrez-partida, E.; Frohloff, L.; Frohna, K.; Mosconi, E.; Radicchi, E.; Lang, F.; Shah, S.; Peña-Camargo, F.; Hempel, H.; Unold, T.; Koch, N.; Armin, A.; De Angelis, F.; Stranks, S.; Neher, D.; Stolterfoht, M. Understanding Performance Limiting Interfacial Recombination in Pin Perovskite Solar Cells. *Adv. Energy Mater.* **2022**, *12*, No. 2103567.

(12) Jiang, K.; Wu, F.; Zhu, L.; Yan, H. Naphthodiperylenetetraimide-Based Polymer as Electron-Transporting Material for Efficient Inverted Perovskite Solar Cells. *ACS Appl. Mater. Interfaces* **2018**, *10* (42), 36549−36555.

(13) Chen, C.; Cheng, M.; Li, H.; Qiao, F.; Liu, P.; Li, H.; Kloo, L.; Sun, L. Molecular Engineering of Ionic Type Perylenediimide Dimer-Based Electron Transport Materials for Efficient Planar Perovskite Solar Cells. *Mater. Today Energy* **2018**, *9*, 264−270.

(14) Jung, S. K.; Heo, J. H.; Lee, D. W.; Lee, S. H.; Lee, S. C.; Yoon, W.; Yun, H.; Kim, D.; Kim, J. H.; Im, S. H.; Kwon, O. P. Homochiral Asymmetric-Shaped Electron-Transporting Materials for Efficient Non-Fullerene Perovskite Solar Cells. *ChemSusChem* **2019**, *12* (1), 224−230.

(15) Jung, S. K.; Heo, J. H.; Lee, D. W.; Lee, S. C.; Lee, S. H.; Yoon, W.; Yun, H.; Im, S. H.; Kim, J. H.; Kwon, O. P. Nonfullerene Electron Transporting Material Based on Naphthalene Diimide Small Molecule for Highly Stable Perovskite Solar Cells with Efficiency Exceeding 20%. *Adv. Funct. Mater.* **2018**, *28* (20), No. 1800346.

(16) Kim, H., Il; Kim, M. J.; Choi, K.; Lim, C.; Kim, Y. H.; Kwon, S. K.; Park, T. Improving the Performance and Stability of Inverted Planar Flexible Perovskite Solar Cells Employing a Novel NDI-Based Polymer as the Electron Transport Layer. *Adv. Energy Mater.* **2018**, *8* (16), No. 1702872.

(17) Zhu, Z.; Zhao, D.; Chueh, C. C.; Shi, X.; Li, Z.; Jen, A. K. Y. Highly Efficient and Stable Perovskite Solar Cells Enabled by All-Crosslinked Charge-Transporting Layers. *Joule* **2018**, *2* (1), 168−183.

(18) Zhao, D.; Zhu, Z.; Kuo, M. Y.; Chueh, C. C.; Jen, A. K. Y. Hexaazatrinaphthylene Derivatives: Efficient Electron-Transporting Materials with Tunable Energy Levels for Inverted Perovskite Solar Cells. *Angew. Chemie - Int. Ed.* **2016**, *55* (31), 8999−9003.

(19) Quinn, J. T. E.; Zhu, J.; Li, X.; Wang, J.; Li, Y. Recent Progress in the Development of N-Type Organic Semiconductors for Organic Field Effect Transistors. *J. Mater. Chem. C* **2017**, *5* (34), 8654−8681.

(20) Bhosale, S. V.; Jani, C. H.; Langford, S. J. Chemistry of Naphthalene Diimides. *Chem. Soc. Rev.* **2008**, *37* (2), 331−342.

(21) Nowak-Król, A.; Shoyama, K.; Stolte, M.; Würthner, F. Naphthalene and Perylene Diimides-Better Alternatives to Fullerenes for Organic Electronics? *Chem. Commun.* **2018**, *54* (98), 13763−13772.

(22) Yan, H.; Lee, P.; Armstrong, N. R.; Graham, A.; Evmenenko, G. A.; Dutta, P.; Marks, T. J. High-Performance Hole-Transport Layers for Polymer Light-Emitting Diodes. Implementation of Organosiloxane Cross-Linking Chemistry in Polymeric Electroluminescent Devices. *J. Am. Chem. Soc.* **2005**, *127* (9), 3172−3183.

(23) Tsai, C. E.; Liao, M. H.; Chen, Y. L.; Cheng, S. W.; Lai, Y. Y.; Cheng, Y. J.; Hsu, C. S. Triarylamine-Based Crosslinked Hole-Transporting Material with an Ionic Dopant for High-Performance PEDOT:PSS-Free Polymer Solar Cells. *J. Mater. Chem. C* **2015**, *3* (24), 6158−6165.

(24) Zuniga, C. A.; Barlow, S.; Marder, S. R. Approaches to Solution-Processed Multilayer Organic Light-Emitting Diodes Based on Cross-Linking. *Chem. Mater.* **2011**, *23* (3), 658−681.

(25) Kawatsuki, N.; Matsuyoshi, K.; Hayashi, M.; Takatsuka, H.; Yamamoto, T. Photoreaction of Photo-Cross-Linkable Methacrylate Polymer Films Comprising 2-Cinnamoyloxyethoxybiphenyl Side Group by Linearly Polarized Ultraviolet Light and Liquid Crystal Alignment on the Resultant Films. *Chem. Mater.* **2000**, *12* (6), 1549−1555.

(26) Gupta, P.; Trenor, S. R.; Long, T. E.; Wilkes, G. L. In Situ Photo-Cross-Linking of Cinnamate Functionalized Poly(methyl methacrylate-*co*-2-hydroxyethyl acrylate) Fibers during Electrospinning. *Macromolecules* **2004**, *37* (24), 9211−9218.

(27) Tremblay, M. H.; Schutt, K.; Zhang, Y.; Lim, J.; Lin, Y. H.; Warby, J. H.; Barlow, S.; Snaith, H. J.; Marder, S. R. A Photo-Crosslinkable Bis-Triarylamine Side-Chain Polymer as a Hole-Transport Material for Stable Perovskite Solar Cells. *Sustain. Energy Fuels* **2020**, *4* (1), 190−198.

(28) Zhang, Y. D.; Hreha, R. D.; Jabbour, G. E.; Kippelen, B.; Peyghambarian, N.; Marder, S. R. Photo-Crosslinkable Polymers as Hole-Transport Materials for Organic Light-Emitting Diodes. *J. Mater. Chem.* **2002**, *12* (6), 1703−1708.

(29) Sung, S. J.; Cho, K. Y.; Hah, H.; Lee, J.; Shim, H. K.; Park, J. K. Two Different Reaction Mechanisms of Cinnamate Side Groups Attached to the Various Polymer Backbones. *Polymer* **2006**, *47* (7), 2314−2321.

(30) Al Kurdi, K.; McCarthy, D. P.; McMeekin, D. P.; Furer, S. O.; Tremblay, M. H.; Barlow, S.; Bach, U.; Marder, S. R. A Naphthalene Diimide Side-Chain Polymer as an Electron-Extraction Layer for Stable Perovskite Solar Cells. *Mater. Chem. Front.* **2021**, *5* (1), 450−457.

(31) Un, H. I.; Gregory, S. A.; Mohapatra, S. K.; Xiong, M.; Longhi, E.; Lu, Y.; Rigin, S.; Jhulki, S.; Yang, C. Y.; Timofeeva, T. V.; Wang, J. Y.; Yee, S. K.; Barlow, S.; Marder, S. R.; Pei, J. Understanding the Effects of Molecular Dopant on N-Type Organic Thermoelectric Properties. *Adv. Energy Mater.* **2019**, *9* (24), No. 1900817.

(32) Kim, M. J.; Lee, M.; Min, H.; Kim, S.; Yang, J.; Kweon, H.; Lee, W.; Kim, D. H.; Choi, J. H.; Ryu, D. Y.; Kang, M. S.; Kim, B. S.; Cho, J. H. Universal Three-Dimensional Crosslinker for All-Photopatterned Electronics. *Nat. Commun.* **2020**, *11* (1), 1520.

(33) Guo, Y.; Sato, W.; Inoue, K.; Zhang, W.; Yu, G.; Nakamura, E. N-Type Doping for Efficient Polymeric Electron-Transporting Layers in Perovskite Solar Cells. *J. Mater. Chem. A* **2016**, *4* (48), 18852−18856.

(34) Chen, H.; Maxwell, A.; Li, C.; Teale, S.; Chen, B.; Zhu, T.; Ugur, E.; Harrison, G.; Grater, L.; Wang, J.; Wang, Z.; Zeng, L.; Park, S. M.; Chen, L.; Serles, P.; Awni, R. A.; Subedi, B.; Zheng, X.; Xiao, C.; Podraza, N. J.; Filleter, T.; Liu, C.; Yang, Y.; Luther, J. M.; De Wolf, S.; Kanatzidis, M. G.; Yan, Y.; Sargent, E. H. Regulating Surface Potential Maximizes Voltage in All-Perovskite Tandems. *Nature* **2023**, *613* (7945), 676−681.

(35) Fürer, S. O.; Rietwyk, K. J.; Pulvirenti, F.; McMeekin, D. P.; Surmiak, M. A.; Raga, S. R.; Mao, W.; Lin, X.; Hora, Y.; Wang, J.; Shi, Y.; Barlow, S.; Ginger, D. S.; Marder, S. R.; Bach, U. Naphthalene-Imide Self-Assembled Monolayers as a Surface Modification of ITO for Improved Thermal Stability of Perovskite Solar Cells. *ACS Appl. Energy Mater.* **2023**, *6* (2), 667−677.

(36) Burgelman, M.; Decock, K.; Khelifi, S.; Abass, A. Advanced Electrical Simulation of Thin Film Solar Cells. *Thin Solid Films* **2013**, *535* (1), 296−301.

(37) Burgelman, M.; Nollet, P.; Degrave, S. Modelling Polycrystalline Semiconductor Solar Cells. *Thin Solid Films* **2000**, *361*, 527−532.

(38) Taddei, M.; Smith, J. A.; Gallant, B. M.; Zhou, S.; Westbrook, R. J. E.; Shi, Y.; Wang, J.; Drysdale, J. N.; McCarthy, D. P.; Barlow, S.; Marder, S. R.; Snaith, H. J.; Ginger, D. S. Ethylenediamine Addition Improves Performance and Suppresses Phase Instabilities in Mixed-Halide Perovskites. *ACS Energy Lett.* **2022**, *7* (12), 4265−4273.

(39) Jin, H.; Farrar, M. D.; Ball, J. M.; Dasgupta, A.; Caprioglio, P.; Narayanan, S.; Oliver, R. D. J.; Rombach, F. M.; Putland, B. W. J.; Johnston, M. B.; Snaith, H. J. Alumina Nanoparticle Interfacial Buffer Layer for Low-Bandgap Lead-in Perovskite Solar Cells. *Adv. Funct. Mater.* **2023**, *33*, No. 2303012.

(40) Zhang, H.; Wang, H.; Chen, W.; Jen, A. K. Y. CuGaO2: A Promising Inorganic Hole-Transporting Material for Highly Efficient and Stable Perovskite Solar Cells. *Adv. Mater.* **2017**, *29* (8), No. 1604984.

(41) Liu, C.; Huang, Z.; Hu, X.; Meng, X.; Huang, L.; Xiong, J.; Tan, L.; Chen, Y. Grain Boundary Modification via F4TCNQ to Reduce Defects of Perovskite Solar Cells with Excellent Device Performance. *ACS Appl. Mater. Interfaces* **2018**, *10* (2), 1909−1916.

(42) Li, Y.; Xu, Z.; Zhao, S.; Song, D.; Qiao, B.; Zhu, Y.; Meng, J. Benefits of the Hydrophobic Surface for $CH_3NH_3PbI_3$ Crystalline Growth towards Highly Efficient Inverted Perovskite Solar Cells. *Molecules* **2019**, *24* (10), 2027.

(43) Lee, J.; Baik, S. Enhanced Crystallinity of $CH_3NH_3PbI_3$ by the Pre-Coordination of PbI_2-DMSO Powders for Highly Reproducible and Efficient Planar Heterojunction Perovskite Solar Cells. *RSC Adv.* **2018**, *8* (2), 1005−1013.

(44) Saliba, M.; Correa-Baena, J. P.; Grätzel, M.; Hagfeldt, A.; Abate, A. Perovskite Solar Cells: From the Atomic Level to Film Quality and Device Performance. *Angew. Chemie - Int. Ed.* **2018**, *57* (10), 2554−2569.

(45) Jariwala, S.; Sun, H.; Adhyaksa, G. W. P.; Lof, A.; Muscarella, L. A.; Ehrler, B.; Garnett, E. C.; Ginger, D. S. Local Crystal Misorientation Influences Non-Radiative Recombination in Halide Perovskites. *Joule* **2019**, *3* (12), 3048−3060.